Molecular Dynamics of Chirality Definable Growth of Single-Walled Carbon Nanotubes

Ryo Yoshikawa[1], Kaoru Hisama[1], Hiroyuki Ukai[1], Yukai Takagi[1], Taiki Inoue[1], Shohei Chiashi[*, 1], Shigeo Maruyama[*, 1, 2]

[1]Deptartment of Mechanical Engineering, The University of Tokyo, 7-3-1 Hongo, Bunkyo-ku, Tokyo 113-8656, Japan
[2]Energy NanoEngineering Laboratory, National Institute of Advanced Industrial Science and Technology (AIST), 1-2-1 Namiki, Tsukuba 305-8654, Japan

[*]E-mail: S. Chiashi: chiashi@photon.t.u-tokyo.ac.jp
[*]E-mail: S. Maruyama: maruyama@photon.t.u-tokyo.ac.jp

ABSTRACT: In order to achieve the chirality-specific growth of single-walled carbon nanotubes (SWCNTs), it is crucial to understand the growth mechanism. Even though many molecular dynamics (MD) simulations have been employed to analyze the SWCNT growth mechanism, it has been difficult to discuss the chirality determining kinetics because of the defects remaining on the SWCNTs grown in simulations. In this study, we demonstrate MD simulations of defect-free SWCNTs, *i.e.* chirality definable SWCNTs, under the optimized carbon supply rate and temperature. The chiralities of the SWCNTs were assigned as (14,1), (15,2), and (9,0), indicating the preference of near-zigzag and pure-zigzag SWCNTs. The SWCNTs contained at least one complete row of defect-free walls consisting of only hexagons. The near-zigzag SWCNTs grew *via* a kink-running process, in which bond formation between a carbon atom at a kink and a neighboring carbon chain led formation of a hexagon with a new kink at the SWCNT edge. Defects including pentagons and heptagons were sometimes formed but effectively healed into hexagons on metal surface. The pure-zigzag SWCNTs grew by the kink-running and the hexagon nucleation processes. In addition, chirality change events along SWCNT with incorporation of pentagon-heptagon pair defects were observed in the MD simulations. Here, pentagons and heptagons were frequently observed as adjacent pairs, resulting in (n,m) chirality changes by (±1,0), (0,±1), (1,-1), or (-1,1).

TOC GRAPHIC

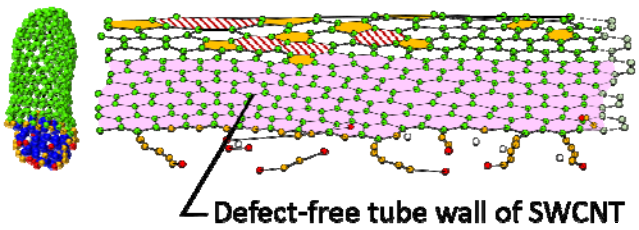

KEYWORDS single-walled carbon nanotubes, molecular dynamics simulation, growth mechanism, lattice defect, metal nanoparticles

Single-walled carbon nanotubes (SWCNTs)[1] have been highly desired for applications in electronic devices because of their tunable band gaps and high carrier mobilities.[2,3] However, semiconducting SWCNTs typically grow as a mixture with metallic SWCNTs.[4] To utilize SWCNTs in semiconducting devices, it is critical to obtain purely semiconducting SWCNTs. While post-growth processes are often applied to separate the semiconducting and metallic SWCNTs,[5–7] these processes can damage and/or contaminate the SWCNTs. Thus, it is preferable to directly synthesize SWCNTs with the specific desirable structures. Many efforts have been made to selectively synthesize semiconducting SWCNTs, particularly SWCNTs with a specific chirality, since chirality determines the electric properties, including the band gap. While considerable experimental progress has been made,[8–10] the clear understanding of the SWCNT growth mechanism is crucial for further improvements of the chirality controlled synthesis.

Numerical simulations and theoretical modellings can be effectively applied to analyze the atomic-scale SWCNT growth mechanism. The theoretical model describing the near armchair preference growth by Yakobson and colleagues[11] ignited the experimental analysis of chiral angle dependence of SWCNT growth[12]. Based on first-principle calculations of SWCNT edges on metal planes, armchair and zigzag structures are energetically more stable than chiral SWCNTs. They ascribe the kink-running growth kinetics as the reason of the departure from pure armchair and pure zigzag.[13] In contrast to the growth kinetics, Bichara and colleagues[14] insisted the preferential growth of chiral SWCNTs with only thermodynamics by formulating the entropy term based on the degeneracy of armchair and zigzag edges on catalyst. On the other hand, Harutyunyan and colleagues[15] argued that cap nucleation process should determine the chirality based on their near zigzag preferential growth experiments from liquid metal catalysts.

Kinetics, which can be studied using molecular dynamics (MD) simulations, should play a role for revealing the mechanisms of growth and chirality determination. Classical MD simulations have previously been employed to observe SWCNT cap formation and growth on Ni and Fe catalysts[16,17] along with the growth of long SWCNTs at high temperature upon lowering the adhesion strength between the cap and catalyst.[18] So far, numerically simulated SWCNTs possess large numbers of defects, and their chiralities could not be discussed. Instead, “local chirality” has been defined based on the diameters and the chiral angles of SWCNTs grown *via* hybrid MD–force biased Monte Carlo simulations[19, 20] and quantum chemical MD simulations.[21] Monte Carlo simulations have been successfully applied to determine the relationship between the carbon solubility of metal nanoparticles and their wettability to graphene and SWCNTs, as well as SWCNT wall growth.[22] A hybrid MD–basin hopping method, a kind of Monte Carlo technique to heal the defects, was used to simulate defect-free SWCNT growth and determine the distribution of chirality.[23] In order to address the chirality determining process, direct MD simulations have been desired that can grow defect-free SWCNTs with definable chirality without artificial defect-healing techniques. For the chirality controlled growth, it is critical to elucidate the time-dependent growth mechanism of SWCNTs, including defect formation and healing processes.

In this study, we successfully observed the growth of chirality-defined SWCNTs using MD simulations with Tersoff-type potential functions[24,25] by optimizing the temperature and the carbon

supply rate in the simulations. Rather than determining the chirality based on the local chiral angle and curvature, the chirality of each SWCNT was evaluated from the configuration of successive hexagons comprising at least one entire row along the SWCNT circumference. The simulations produced both pure-zigzag and near-zigzag types of SWCNTs. The atomic-scale growth mechanism involved the formation of hexagonal carbon rings through the kink running accompanied by the formation and healing of defects. The incorporation of pairs of pentagons and heptagons, resulting in a change in SWCNT chirality, was also observed.

RESULTS & DISCUSSION

Molecular Dynamics Growth of Chirality Definable SWCNTs

We observed defect-free SWCNT growth, defective SWCNT growth, and failure of SWCNT growth in the MD simulations (Fig. S2), depending on the growth temperature and carbon supply. Figure 1 shows three SWCNTs with defect-free walls grown in MD simulations at (a) T = 1550 K on Co catalyst, (b) T = 1400 K during cap nucleation, and T = 1600 K during wall growth on Co catalyst, and (c) T = 1200 K on Fe catalyst. All defect-free walls were grown at n^* = 1 (low pressure). By directly tracing rows of hexagons, the chiralities of the SWCNTs were determined to be (14,1),

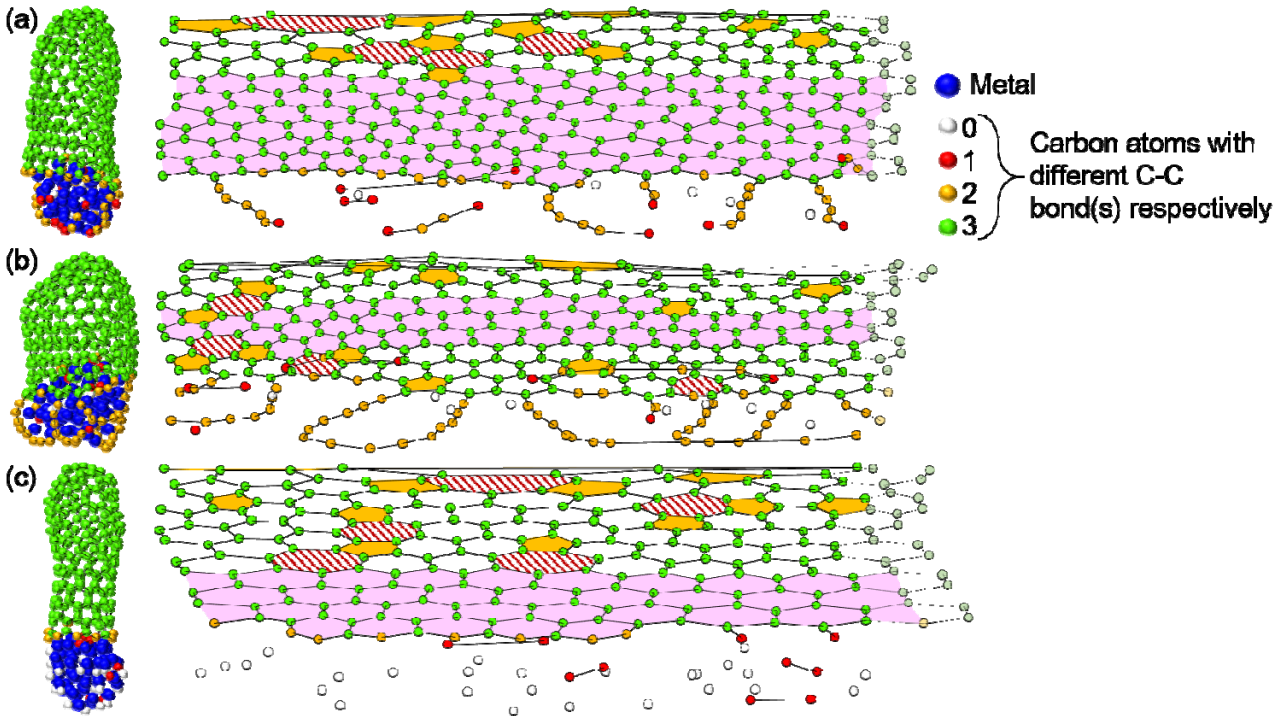

Fig. 1. Snapshots and development views of defect-free SWCNTs grown by MD simulation. (a) (14,1) SWCNT from 60-mer Co at 1550 K, 840 ns. (b) (15,2) SWCNT from 60-mer Co, at 1400 K (0–360 ns, cap formation) and at 1600 K (360–780 ns, wall growth), 780 ns. (c) (9,0) SWCNT from 60-mer Fe at 1200 K, 501 ns. Metal atoms in the development views were omitted for clarity. The orange-filled and red-striped areas are pentagons and heptagons, respectively. The areas in pink are the defect-free walls composed of successive hexagons.

(15,2) on the Co catalyst and (9,0) on the Fe catalyst. Generally, a perfect SWCNT cap contains six pentagons and no heptagons. In contrast, defective caps contain at least one heptagon, and the number of pentagons are always six plus number of heptagons so as to satisfy the geometric requirement. The SWCNT caps grown in this study were not perfect, but satisfied the isolated pentagon rule.[26,27]

Growth Modes Depending on the Catalyst Species

For the Co catalysts, the long carbon chains on their edges are apparent as shown in Figs. 1(a) and (b). For the case of Fe catalysts, the carbon chains have also important roles, even though they are very short and volatile. This difference is derived from the different strength of the interaction between sp carbon atoms and the catalyst[25]. The carbon chains, including the short ones, have mainly two roles. One is the precursors of the newly formed hexagons as noted in the next chapter, and the other is bridges between the SWCNTs and the catalysts to prevent SWCNTs from detaching from the catalysts. Since the carbon chains on the Fe catalysts are short and volatile, they are sometimes too weak to play the latter role, resulting in cap detachment from the catalyst (see Fig. S1 (a) in the supporting information). Then, we conclude that all the SWCNTs had carbon chains on their edges where they attached to the catalysts. Unlike the carbon chains on the Fe catalyst, which appeared and disappeared over time, the carbon chains on the Co catalyst prevailed throughout the simulations. This growth mode, in which carbon chains are persistently present on the Co catalyst like octopus tentacles, is termed “octopus mode.” In octopus mode, the carbon chains move on the surface of the Co catalyst and contribute to SWCNT growth, as discussed in more detail below. Compared to the octopus mode of growth observed on the Co catalyst, the SWCNTs on the Fe catalyst exhibited volatile, fewer and shorter chains (non-octopus mode). This difference is attributed to the difference in interaction strength between the catalysts and carbon chains.[25] Moreover, the SWCNTs on Co catalysts had larger diameters than those on Fe catalysts. For example, the values of the diameter ratio of the SWCNT/catalyst are 0.81 in the (14,1) SWCNT on Co catalyst and 0.64 in the (9,0) SWCNT on Fe catalyst, which means that a closer match of diameters is observed in octopus mode on Co catalyst than in non-octopus mode on Fe catalyst. Despite the long-time simulation, the diameter ratios were almost constant during the growth. This catalyst dependence of the diameter ratios is also observed in the cases of defective tubes. Fe nanoparticles in this system dissolved more carbon atoms during constant growth (representatively 27 carbon atoms in 60-mer Fe) than Co nanoparticles (representatively 19 carbon atoms in 60-mer Co.) Apparently, the difference is consistent with He, *et al.*, (2018),[28] that claims more carbon solubility leads to smaller SWCNT diameter *versus* nanoparticle diameter ratio. In addition, Co catalysts deformed into elongated shapes to the radial direction of SWCNT. It can be understood that the initial part of cap starting from the metal catalyst ended up with a tube that had slightly larger diameter than the catalyst and at the same time stretched the catalyst. In a previous report, two growth modes were observed using transmission electron microscopy: a tangential mode, where the SWCNT diameter is similar to the catalyst diameter; and a perpendicular growth mode, where the SWCNT diameter is smaller than the catalyst diameter.[29] Octopus mode on the Co catalyst in this MD system is considered to correspond to the

tangential growth in terms of the diameter ratio of SWCNT and catalyst, while non-octopus mode on the Fe catalyst could be similar to the perpendicular growth.

Because the growth on the Fe catalyst corresponds to the perpendicular mode discussed in Fiawoo, *et al.*,[29] we compared Gibbs free energy map[14] in Fig. S2 in the supporting information. It can be understood that pure-zigzag SWCNTs grow continuously because zigzag edge is more stable than armchair edge. In the cases of the Co catalyst, the SWCNT edges contained predominantly zigzag structure. There is an experimental report of near-zigzag preferential growth.[15] However, there are more experimental reports of near-armchair preferential growth.[30–33] Near-armchair preferential growth or stability of armchair edge compared with zigzag edge can be attributed to the incomplete pi electron conjugation or in other words the incomplete resonance in zigzag edge, which cannot be described by Brenner-Tersoff potential. It can be understood that these tendency of diameter ratio and the zigzag preference determined the chiralities, (14,1), (15,2) and (9,0).

Dynamics of Kinks and Carbon Chains

We observed dynamic roles of kinks and carbon chains at SWCNT edges for the formation of hexagons. Figure 2 shows the detailed growth process of the (14,1) SWCNTs [Fig. 1(a)]. During the majority of the period of the growth process, a kink runs along the zigzag edge, as shown in Fig. 2(a).

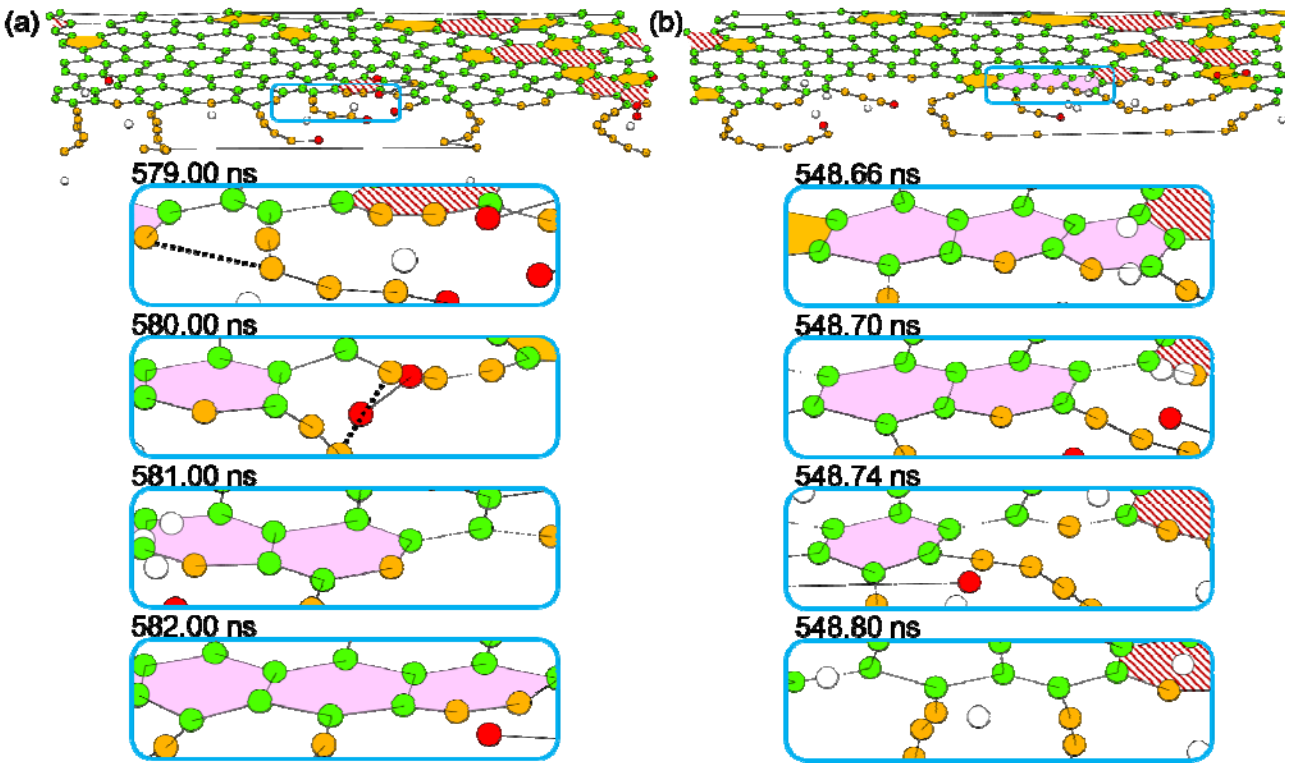

Fig. 2. Growth process of near-zigzag (14,1) SWCNT. (a) Kink-running process. A bond formation between a carbon atom on the kink and another atom in the carbon chain results in the appearance of a new hexagon with two kink sites. The dot lines indicate the carbon atoms that are about to bond each other to make the new hexagons in the following time steps. (b) Process of reverse kink running. Hexagons are decomposed into carbon chains.

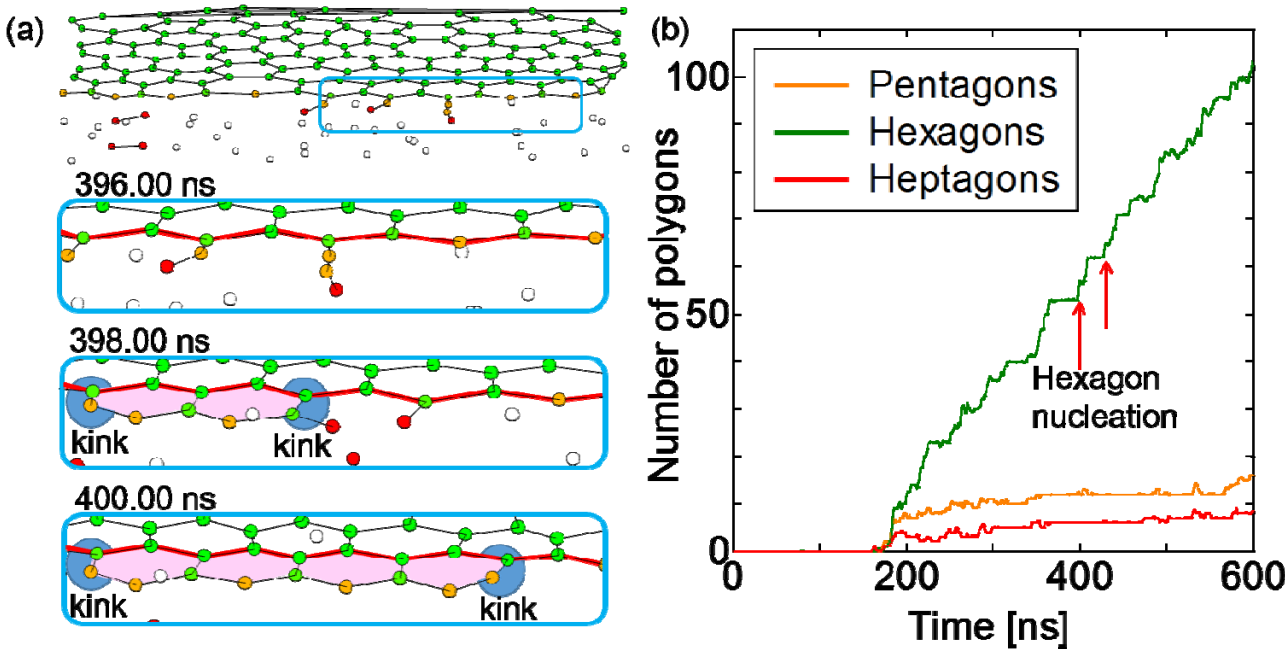

Fig. 3. Growth process of pure-zigzag (9,0) SWCNT. (a) Hexagon nucleation process. After the formation of one complete ring of hexagons, an extra hexagon with a pair of kinks appears. Then, the kink-running process is initiated. (b) Time evolution of the number of pentagons, hexagons, and heptagons. The arrows show the time when the extra hexagon nucleation occurred. Following the hexagon nucleation, the smooth increase of nine hexagons was observed.

An atom in the kink bonds to an atom in the neighboring carbon chain, forming a new hexagon with a new kink as its side. Sometimes, the reverse reaction process was observed, as shown in Fig. 2(b). In this reaction process, hexagons were destroyed, leaving carbon chains.

In the case of pure-zigzag-type, (9,0) SWCNTs shown in Figure 3, a pair of zigzag kinks disappeared each time that a ring (row of hexagons) was formed. Thus, unlike for chiral (14,1) SWCNTs, the kink-running process alone cannot describe the growth. An additional hexagon nucleation process, in which a new pair of kinks appears on the edge of a zigzag SWCNT, was also involved in SWCNT growth [Fig. 3 (a)].[11,34] This reaction process was caused by very short carbon chains consisting of one or two carbon atom(s). An atom on a carbon chain and a separate atom on another carbon chain bonded together to form a new hexagon, and both sides of the hexagon became a new pair of kinks. The formation of the complete ring along the circumference of the SWCNT and the formation of a new hexagon on a complete ring were separated by a short period of time. The pair of kinks ran in the opposite direction and finally bonded together, resulting in an absence of kinks. Figure 3(b) shows the time evolution of the numbers of pentagons, hexagons, and heptagons on a (9,0) SWCNT. The results indicate that the SWCNT growth was suspended until the next hexagon was nucleated, as mentioned above. This delay in growth suggests that the energy barrier to a new hexagon creation (accompanied with 2 kinks) is larger than that of the kink-running reaction, which is consistent with the experimental difficulty in selectively growing pure-zigzag SWCNTs.[35]

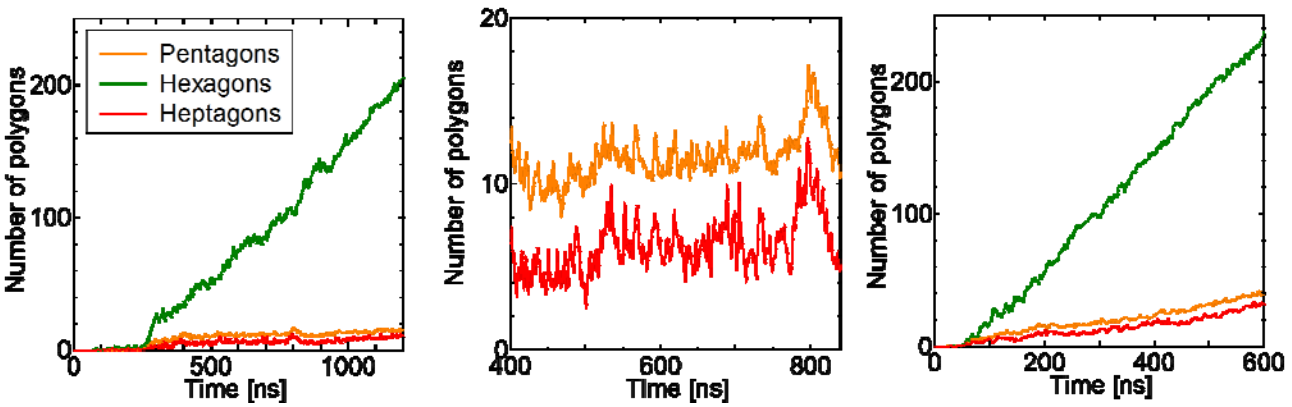

Fig. 4. Time evolution of the numbers of pentagons, hexagons, and heptagons. (a) Defect-free SWCNT growth under $n^* = 1$. (b) An enlarged view of (a). (c) Defective SWCNT growth under $n^* = 3$. Both cases are at $T = 1550$ K on the 60-mer Co catalysts.

Pentagon and Heptagon Defect Formation and Chirality Change

In addition to hexagons, the kink-running reaction can also form defects, including pentagons and heptagons. Nevertheless, defect-free SWCNTs continued to be formed because of the defect-healing process on their edge, especially on the Co catalyst. Figure 4 compares the time evolution of the numbers of pentagons, hexagons, and heptagons between defect-free growth ($n^* = 1$) and defective growth ($n^* = 3$) at $T = 1550$ K on 60-mer Co catalysts. For defect-free growth, the number of pentagons and heptagons remained constant [Figs. 4(a) and (b)] over time; in contrast, for defective growth, the number of these defects increased with time [Fig. 4(c)]. The fluctuation in the number of defects shown in Figs. 4(a) and (b) indicates that defects were formed even in the case of defect-free growth but were healed into hexagons. In fact, the heptagons and pentagons were occasionally mediated by carbon chains, converting them into hexagons [Figs. 5(a) and (b)]. The pairs of adjacent pentagons and heptagons along the tube edge were more efficiently healed into two hexagons as shown in Fig. 5(c). The fully correlated fluctuations of the number of pentagons and the

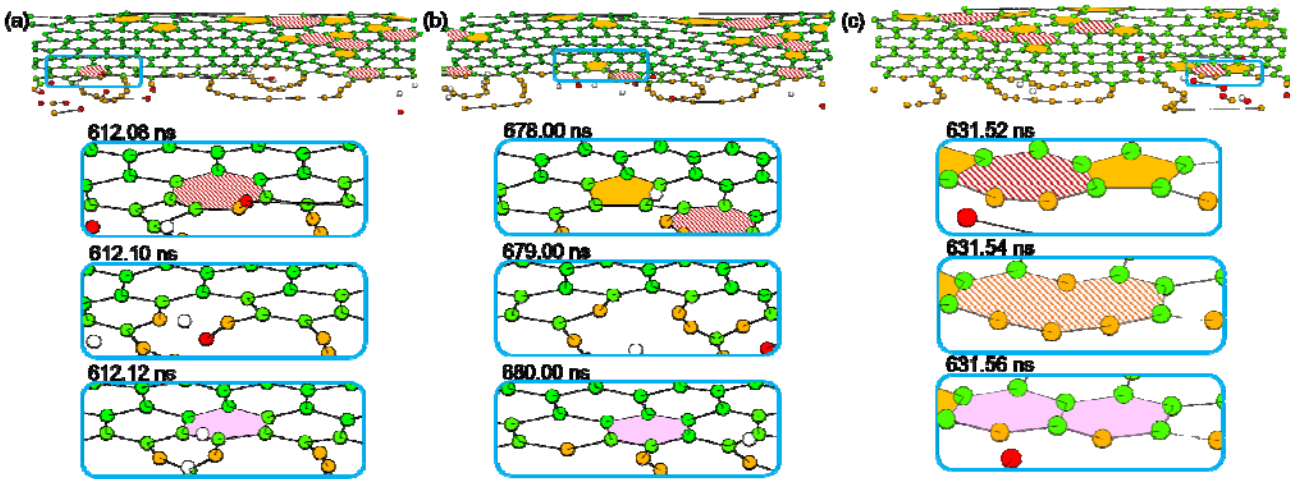

Fig. 5. Edge healing processes of the (14,1) SWCNT. All of the processes occurred only on the catalyst metal particle. (a) Reformation of a heptagon into a hexagon. (b) Reformation of a pentagon into a hexagon. (c) Transformation of a pentagon-heptagon pair into two hexagons.

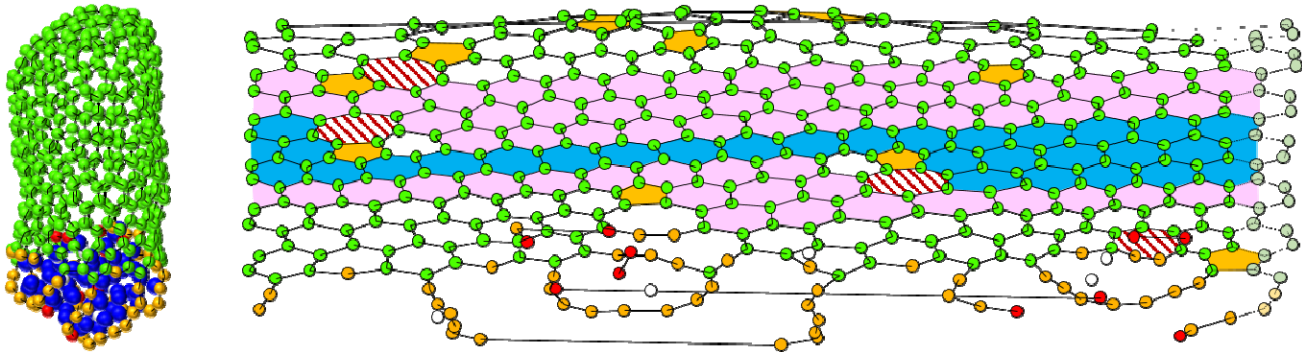

Fig. 6. Snapshot and development view of an SWCNT with a defect-mediated chirality junction of (15,2) and (16,2) grown from 60-mer Co at 1400 K (until 360 ns, cap formation) and 1600 K (after 360 ns, wall growth), 960ns. The orange and the red-striped polygons are pentagons and heptagons, respectively. The pink and blue parts are (15,2) and (16,2) defect-free walls, respectively.

number of heptagons in Fig. 4 (b) can be interpreted as that pentagon appearing/disappearing often coincides with heptagon appearing/disappearing. This means that single pentagon or heptagon per row can remain which leads to the tube-axis-alignment of defects. These processes of defect healing was observed only at the edges of the SWCNTs as a result of the decreased energy barriers caused by the catalyst.[36] These kink-running and defect-healing processes contributed to the growth of defect-free SWCNT walls.

Finally, we discuss the change in chirality observed during the further growth process of SWCNT as shown in Fig. 6. The (15,2) SWCNTs maintained defect-free growth for several rows followed by the formation of defect structures, causing the chirality to change to (16,2) (Fig. S4). Subsequently, the SWCNT chirality again changed back to (15,2). Each change in chirality occurred in conjunction with a pair of pentagons and heptagons.[37–39] We also observed a chirality change of an SWCNT from (14,1) to (10,2) with three pairs of pentagons and heptagons (not shown). An adjacent pair of one pentagon and one heptagon changes the chirality by (±1,0), (0,±1), (1,-1), or (-1,1); the greater the distance between the pentagon and heptagon, the larger the change in chirality.[40] In our MD simulations, each heptagon tended to be located near to a pentagon, and adjacent pairs were the most common, as observed experimentally in graphene grain boundaries.[41]

CONCLUSIONS

We successfully simulated the growth of three defect-free SWCNTs, (14,1), (15,2), and (9,0), using MD simulations with a low carbon supply rate. The (14,1) and (15,2) SWCNTs grew on Co catalysts in octopus mode *via* a kink-running process with edge healing. The (9,0) SWCNTs grew on Fe catalysts in non-octopus mode. During the growth of zigzag (9,0) SWCNTs, a nucleation of hexagon with two kinks was observed in addition to kink running. The periodic emergence of the kinks permitted growth of pure-zigzag tube, in accord with analytical results of Artyukhov, *et al.*[13] (Eq. 2 and Fig. 3d in reference 13). All growth processes occurred on metal catalyst particles *via* reactions between carbon chains and SWCNT edges. During growth, the (15,2) SWCNTs changed to (16,2)

SWCNTs with junctions consisting of adjacent pairs of pentagons and heptagons. These observations of atomic-scale, time-dependent SWCNT growth processes should contribute to our understanding of how SWCNT chirality is determined, together with other simulations, experiments, and theories.

METHODS

Classical MD simulations using potential functions derived from density functional theory (DFT) were performed to reproduce SWCNT growth. Compared to direct DFT simulations, classical MD simulations are far more computationally inexpensive and are therefore suitable for simulating the entire growth process of SWCNTs over a long time scale.

A metal nanoparticle consisting of 60 atoms of Co or Fe was placed at the center of a $10\times10\times10$-nm^3 cubic cell under periodic boundary conditions along all the three axes. The metal nanoparticle was at first placed as a simple cubic structure and then tuned into a spherical cluster by annealing at 1500 K for 2 ns. The following potential functions were used to describe the interactions among the atoms: Tersoff-type potentials[25] for metal–metal and metal–carbon bonds; modified Brenner–Tersoff potentials[26,16] for chemically bound carbon atoms; and Lennard–Jones potentials for the interactions between distant non-covalent carbon atoms. The Tersoff-type potential functions were constructed by fitting the dissociation energies and lattice constants of metal–carbon lattices (*e.g.*, NaCl-type, CsCl-type, and zinc blende-type structures) determined by DFT calculation.[24,25] A Nosé–Hoover thermostat[43,44] was applied only for metal nanoparticles to maintain the temperature of the system at T. The velocity Verlet algorithm with time step $\Delta t = 0.5$ fs was applied for numerical integration.

Carbon atoms were supplied into the cell to grow SWCNTs. The starting positions and directions of the initial velocities of the carbon atoms were randomly assigned. The initial speeds were constant, assuming the temperature of the system was T. Once in the time period $\Delta t_{\mathrm{supply}}$, no or one carbon atom were supplied to the cell so that the density of free carbon remained constant at n. Here, $\Delta t_{\mathrm{supply}}$ and n correspond together to the pressure of the carbon source (or chemical potential), and the set of two variables determine the mean density of free carbon, n^*. The definition of $\Delta t_{\mathrm{supply}}$ and n may be suspected to be quite redundant. However, the use of $\Delta t_{\mathrm{supply}}$ is practically very convenient for achieving the enough relaxation time. For Co catalyst, simulations were conducted at $T = 1300$–1600 K in 50-K increments and $n^* = 1$ or 3. For Fe catalyst, simulations were conducted at $T = 1000$–1500 K in 50-K increments and $n^* = 1$. All simulations were repeated several times under the same conditions.

We propose the development views of SWCNTs to clarify the crystal structures of the tube wall and carbon-metal interfaces. Considering a cylindrical coordinate system in which a line connecting the centroid of the catalyst with that of the SWCNT is the z axis, each (r, θ, z) point was placed at (θ, z) on the developed plane.

The chirality of each SWCNT was determined based on one whole row of hexagons that can be traced along the positive combination of $\boldsymbol{a}_1$ and $\boldsymbol{a}_2$ vectors, which are the basis vectors of a

graphene sheet of a developed SWCNT. More information on the determination of chirality can be found in the Supporting Information.

ASSOCIATED CONTENT

Supporting Information. The Supporting Information is available free of charge on the ACS Publications website. It contains the details of CNT growth failure, the contour plot of Fe (1 1 1) plane-SWCNT interfacial energy, the definition of "chirality-definable," the diagram of the junction between (15,2) and (16,2) SWCNTs, and animation movies of the growth processes of the (14,1) and the (9,0) SWCNTs.

AUTHOR INFORMATION

Corresponding Authors

*E-mail: S. Chiashi: chiashi@photon.t.u-tokyo.ac.jp

*E-mail: S. Maruyama: maruyama@photon.t.u-tokyo.ac.jp

Author Contributions

R.Y., S.C. and S.M. conceived the project. R.Y., K.H., H.U. and Y.T. carried out all simulations. R.Y., K.H., T.I., S.C. and S.M. analyzed the data. R.Y. and T.I. cowrote the manuscript. All the authors discussed the results and commented on the manuscript.

Notes

The authors declare no competing financial interest.

ACKNOWLEDGMENTS

Part of this work was financially supported by JSPS KAKENHI Grant Numbers JP15H05760, JP17K06187, and JP18H05329.

REFERENCES

1. Iijima, S.; Ichihashi, T. Single-Shell Carbon Nanotubes of 1-Nm Diameter. *Nature* **1993**, *363* , 603–605.
2. Dürkop, T.; Getty, S. A.; Cobas, E.; Fuhrer, M. S. Extraordinary Mobility in Semiconducting Carbon Nanotubes. *Nano Lett.* **2004**, *4* , 35–39.
3. Perebeinos, V.; Tersoff, J.; Avouris, P. Mobility in Semiconducting Carbon Nanotubes at Finite Carrier Density. *Nano Lett.* **2006**, *6* , 205–208.

4. Telg, H.; Maultzsch, J.; Reich, S.; Hennrich, F.; Thomsen, C. Chirality Distribution and Transition Energies of Carbon Nanotubes. *Phys. Rev. Lett.* **2004**, *93* , 1–4.
5. Arnold, M. S.; Green, A. A.; Hulvat, J. F.; Stupp, S. I.; Hersam, M. C. Sorting Carbon Nanotubes by Electronic Structure Using Density Differentiation. *Nat. Nanotechnol.* **2006**, *1* , 60–65.
6. Tu, X.; Manohar, S.; Jagota, A.; Zheng, M. DNA Sequence Motifs for Structure-Specific Recognition and Separation of Carbon Nanotubes. *Nature* **2009**, *460* , 250–253.
7. Liu, H.; Nishide, D.; Tanaka, T.; Kataura, H. Large-Scale Single-Chirality Separation of Single-Wall Carbon Nanotubes by Simple Gel Chromatography. *Nat. Commun.* **2011**, *2* , 308–309.
8. Zhou, W.; Zhan, S.; Ding, L.; Liu, J. General Rules for Selective Growth of Enriched Semiconducting Single Walled Carbon Nanotubes with Water Vapor as *In Situ* Etchant. *J. Am. Chem. Soc.* **2012**, *134* , 14019–14026.
9. Yang, F.; Wang, X.; Zhang, D.; Yang, J.; Luo, D.; Xu, Z.; Wei, J.; Wang, J.-Q.; Xu, Z.; Peng, F.; Li, X.; Li, R.; Li, Y.; Li, M.; Bai, X.; Ding, F.; Li, Y. Chirality-Specific Growth of Single-Walled Carbon Nanotubes on Solid Alloy Catalysts. *Nature* **2014**, *510* , 522–524.
10. Zhang, S.; Kang, L.; Wang, X.; Tong, L.; Yang, L.; Wang, Z.; Qi, K.; Deng, S.; Li, Q.; Bai, X.; Ding, F.; Zhang, J. Arrays of Horizontal Carbon Nanotubes of Controlled Chirality Grown Using Designed Catalysts. *Nature* **2017**, *543* , 234–238.
11. Ding, F.; Harutyunyan, A. R.; Yakobson, B. I. Dislocation Theory of Chirality-Controlled Nanotube Growth. *Proc. Natl. Acad. Sci. U. S. A.* **2009**, *106* , 2506–2509.
12. Rao, R.; Liptak, D.; Cherukuri, T.; Yakobson, B. I.; Maruyama, B. *In Situ* Evidence for Chirality-Dependent Growth Rates of Individual Carbon Nanotubes. *Nat. Mater.* **2012**, *11* , 213–216.
13. Artyukhov, V.; Penev, E.; Yakobson, B. Why Nanotubes Grow Chiral. *Nat. Commun.* **2014**, *5* (May), 1–6.
14. Magnin, Y.; Amara, H.; Ducastelle, F.; Loiseau, A.; Bichara, C. Entropy-Driven Stability of Chiral Single-Walled Carbon Nanotubes. *Science* **2018**, *362* , 212–215.
15. Pierce, N.; Chen, G.; Rajukumar, L. P.; Chou, N. H.; Koh, A. L.; Sinclair, R.; Maruyama, S.; Terrones, M.; Harutyunyan, A. R. Intrinsic Chirality Origination in Carbon Nanotubes. *ACS Nano* **2017**, *11* , 9941–9949.
16. Shibuta, Y.; Maruyama, S. Molecular Dynamics Simulation of Formation Process of Single-Walled Carbon Nanotubes by CCVD Method. *Chem. Phys. Lett.* **2003**, *382* (3–4), 381–386.
17. Ding, F.; Bolton, K.; Rosén, A. Nucleation and Growth of Single-Walled Carbon Nanotubes: A Molecular Dynamics Study. *J. Phys. Chem. B* **2004**, *108* , 17369–17377.
18. Ribas, M. A.; Ding, F.; Balbuena, P. B.; Yakobson, B. I. Nanotube Nucleation *versus* Carbon-Catalyst Adhesion-Probed by Molecular Dynamics Simulations. *J. Chem. Phys.* **2009**, *131* , 224501.
19. Neyts, E. C.; Shibuta, Y.; van Duin, A. C. T.; Bogaerts, A. Catalyzed Growth of Carbon Nanotube with Definable Chirality by Hybrid Molecular Dynamics−Force Biased Monte Carlo Simulations. *ACS Nano* **2010**, *4* , 6665–6672.
20. Neyts, E. C.; van Duin, A. C. T.; Bogaerts, A. Changing Chirality during Single-Walled Carbon Nanotube Growth: A Reactive Molecular Dynamics/Monte Carlo Study. *J. Am. Chem. Soc.* **2011**, *133* , 17225–17231.
21. Kim, J.; Page, A. J.; Irle, S.; Morokuma, K. Dynamics of Local Chirality during SWCNT Growth: Armchair *versus* Zigzag Nanotubes. *J. Am. Chem. Soc.* **2012**, *134* , 9311–9319.
22. Diarra, M.; Zappelli, A.; Amara, H.; Ducastelle, F.; Bichara, C. Importance of Carbon Solubility and Wetting Properties of Nickel Nanoparticles for Single Wall Nanotube Growth. *Phys. Rev. Lett.* **2012**, *109* , 185501.
23. Xu, Z.; Yan, T.; Ding, F. Atomistic Simulation of the Growth of Defect-Free Carbon Nanotubes. *Chem. Sci.* **2015**, *6* , 4704–4711.
24. Kumagai, T.; Hara, S.; Izumi, S.; Sakai, S. Development of a Bond-Order Type Interatomic Potential for Si–B Systems. *Model. Simul. Mater. Sci. Eng.* **2006**, *14* , S29–S37.
25. Hisama, K.; Yoshikawa, R.; Matsuo, T.; Noguchi, T.; Kawasuzuki, T.; Chiashi, S.; Maruyama, S. Growth Analysis of Single-Walled Carbon Nanotubes Based on Interatomic Potentials by Molecular Dynamics Simulation. *J. Phys. Chem. C* **2018**, *122* , 9648–9653.
26. Brinkmann, G.; Fowler, P.; Manolopoulos, D. .; Palser, A. H. . A Census of Nanotube Caps. *Chem. Phys. Lett.* **1999**, *315*, 335–347.
27. Reich, S.; Li, L.; Robertson, J. Structure and Formation Energy of Carbon Nanotube Caps. *Phys. Rev. B* **2005**, *72* , 165423.
28. He, M.; Magnin, Y.; Jiang, H.; Amara, H.; Kauppinen, E. I.; Loiseau, A.; Bichara, C. Growth Modes and Chiral Selectivity of Single-Walled Carbon Nanotubes. *Nanoscale* **2018**, *10* , 6744–6750.
29. Fiawoo, M. F. C.; Bonnot, A. M.; Amara, H.; Bichara, C.; Thibault-Pénisson, J.; Loiseau, A. Evidence of Correlation between Catalyst Particles and the Single-Wall Carbon Nanotube Diameter: A First Step towards Chirality Control. *Phys. Rev. Lett.* **2012**, *108*, 195503.
30. Lolli, G.; Zhang, L.; Balzano, L.; Sakulchaicharoen, N.; Tan, Y.; Resasco, D. E. Tailoring (n,m) Structure of Single-Walled Carbon Nanotubes by Modifying Reaction Conditions and the Nature of the Support of CoMo Catalysts. *J. Phys. Chem. B* **2006**, *110* , 2108–2115.

31. He, M.; Jiang, H.; Kauppinen, E. I.; Lehtonen, J. Diameter and Chiral Angle Distribution Dependencies on the Carbon Precursors in Surface-Grown Single-Walled Carbon Nanotubes. *Nanoscale* **2012**, *4* , 7394–7398.
32. He, M.; Jiang, H.; Liu, B.; Fedotov, P. V.; Chernov, A. I.; Obraztsova, E. D.; Cavalca, F.; Wagner, J. B.; Hansen, T. W.; Anoshkin, I. V.; Obraztsova, E. A.; Belkin, A. V.; Sairanen, E.; Nasibulin, A. G.; Lehtonen, J.; Kauppinen, E. I. Chiral-Selective Growth of Single-Walled Carbon Nanotubes on Lattice-Mismatched Epitaxial Cobalt Nanoparticles. *Sci. Rep.* **2013**, *3*, 1–7.
33. Wang, H.; Wang, B.; Quek, X. Y.; Wei, L.; Zhao, J.; Li, L. J.; Chan-Park, M. B.; Yang, Y.; Chen, Y. Selective Synthesis of (9,8) Single Walled Carbon Nanotubes on Cobalt Incorporated TUD-1 Catalysts. *J. Am. Chem. Soc.* **2010**, *132* , 16747–16749.
34. Yuan, Q.; Ding, F. How a Zigzag Carbon Nanotube Grows. *Angew. Chemie - Int. Ed.* **2015**, *54* , 5924–5928.
35. Yang, F.; Wang, X.; Zhang, D.; Qi, K.; Yang, J.; Xu, Z.; Li, M.; Zhao, X.; Bai, X.; Li, Y. Growing Zigzag (16,0) Carbon Nanotubes with Structure-Defined Catalysts. *J. Am. Chem. Soc.* **2015**, *137* , 8688–8691.
36. Yuan, Q.; Xu, Z.; Yakobson, B. I.; Ding, F. Efficient Defect Healing in Catalytic Carbon Nanotube Growth. *Phys. Rev. Lett.* **2012**, *108* , 245505.
37. Yao, Z.; Postma, H. W. C.; Balents, L.; Dekker, C. Carbon Nanotube Intramolecular Junctions. *Nature* **1999**, *402* , 273–276.
38. Otsuka, K.; Yamamoto, S.; Inoue, T.; Ukai, H.; Yoshikawa, R.; Xiang, R.; Chiashi, S.; Maruyama, S. Digital Isotope Coding to Trace Growth Process of Individual Single-Walled Carbon Nanotubes. *ACS Nano* **2018**, *12* , 3994–4001.
39. Yakobson, B. I. Mechanical Relaxation and “Intramolecular Plasticity” in Carbon Nanotubes. *Appl. Phys. Lett.* **1998**, *72* , 918–920.
40. Saito, R.; Dresselhaus, G.; Dresselhaus, M. S. *Physical Properties of Carbon Nanotubes*; Imperial College Press, 1998.
41. Rasool, H. I.; Ophus, C.; Zhang, Z.; Crommie, M. F.; Yakobson, B. I.; Zettl, A. Conserved Atomic Bonding Sequences and Strain Organization of Graphene Grain Boundaries. *Nano Lett.* **2014**, *14*, 7057–7063.
42. Brenner, D. W. Empirical Potential for Hydrocarbons for Use in Simulating the Chemical Vapor Deposition of Diamond Films. *Phys. Rev. B* **1990**, *42* , 9458–9471.
43. Nose, S. A Unified Formulation of the Constant Temperature Molecular Dynamics Methods. *J. Chem. Phys.* **1984**, *81*, 511–519.
44. Hoover, W. G. Canonical Dynamics: Equilibrium Phase-Space Distributions. *Phys. Rev. A* **1985**, *31*, 1695–1697.

Supporting Information for:

Molecular Dynamics of Chirality Definable Growth of Single-Walled Carbon Nanotubes

Ryo Yoshikawa[1], Kaoru Hisama[1], Hiroyuki Ukai[1], Yukai Takagi[1], Taiki Inoue[1], Shohei Chiashi[*, 1], Shigeo Maruyama[*, 1, 2]

[1]Deptartment of Mechanical Engineering, The University of Tokyo, 7-3-1 Hongo, Bunkyo-ku, Tokyo 113-8656, Japan
[2]Energy NanoEngineering Laboratory, National Institute of Advanced Industrial Science and Technology (AIST), 1-2-1 Namiki, Tsukuba 305-8654, Japan

1. Various Simulation Results

We tried 13 different temperature and 2 different carbon supply rate. The all conditions are shown in Table. S2. Depending on the temperature and the carbon supply rate, we observed various growth failures in our simulations as in Fig. S2. Graphene encapsulation (Fig. S1 (a)) was quite often observed on the Co catalyst at lower temperature (T < 1350 K), carbon chain coil (Fig. S1 (b)) was often observed on the Co catalyst at higher temperature (T > 1500 K) under lower carbon supply (n^* = 1). The other two were observed on the Fe catalyst. SWCNT-like amorphous carbon growth (Fig. S1 (c)) was observed at lower temperature (T < 1100 K) and fullerene detachment (Fig. S1 (d)) was observed at higher temperature (T > 1200 K).

Table. S1. All simulation conditions and results. Circles mean defective SWCNT growth, and stars mean defect-free SWCNT growth. a to d mean growth failure and correspond to (a) to (d) in Fig S1.

Catalyst	n^*	1300 K	1350 K	1400 K	1450 K	1500 K	1550 K	1600 K
60-mer Co	1	a	○	○	○	○	☆, b	☆, b
60-mer Co	3	a	○	○	○	○	○	○
Catalyst	n^*	1000 K	1050 K	1100 K	1150 K	1200 K	1250 K	1300 K
60-mer Fe	1	○	○, c	○	○	☆, d	d	d

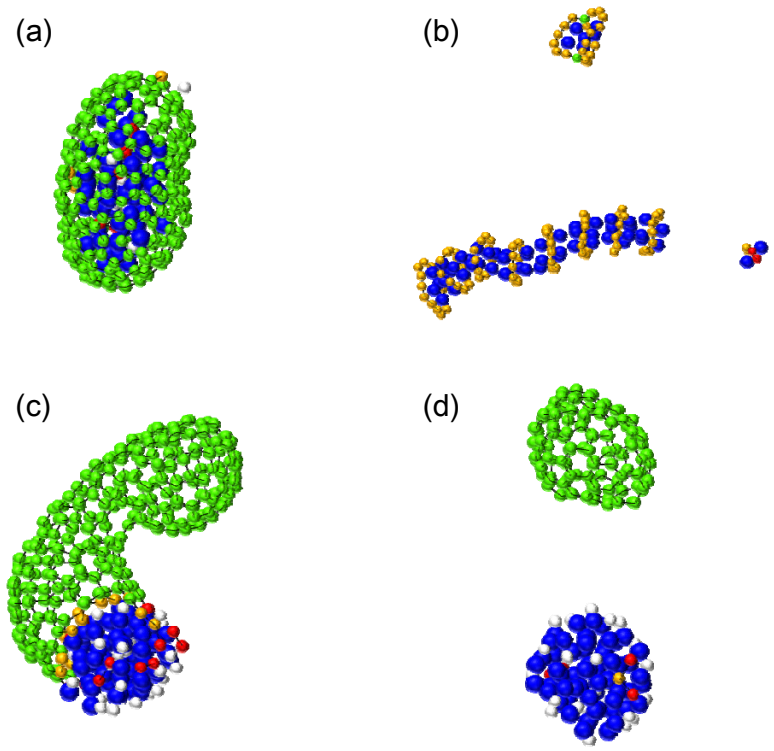

Fig. S1. SWCNT growth failures. (a) Graphene encapsulation. (b) Carbon chain coil. (c) Amorphous carbon. (d) Fullerene.

2. Energetic Stability of the SWCNT Edge and Zigzag Preference

In our simulation results, near- and pure-zigzag SWCNTs grew. Here, the origin of zigzag preference is examined by calculating the energetic stability of SWCNT edge. On Fe catalysts, the SWCNTs grew in perpendicular mode, and therefore the method of measuring Gibbs free energy of the edge[1] can be applied. Interfacial energies between SWCNTs and Fe (1 1 1) plane are shown in Table. S1.

Table. S2. Interfacial energy between SWCNTs and Fe (1 1 1) plane.

n	m	Interfacial Energy [eV]
6	5	-5.445
8	4	-7.810
9	1	-9.292
10	0	-8.402

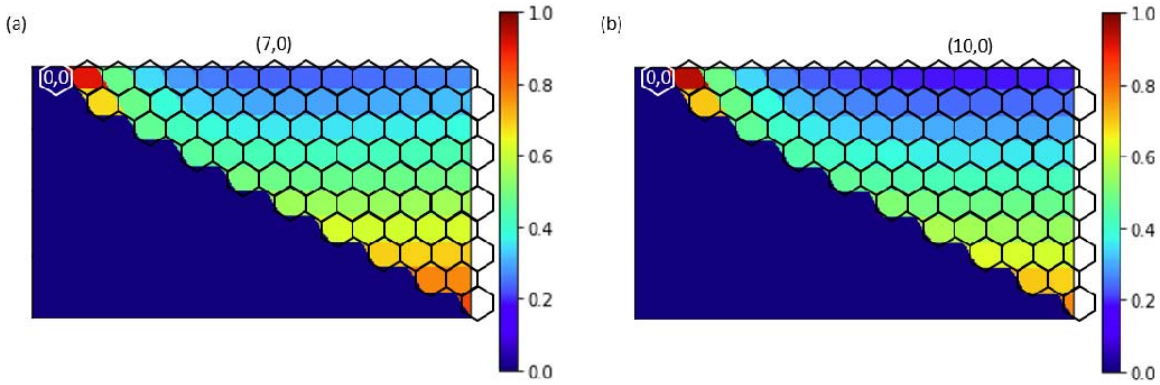

Fig. S2. Relative Gibbs free energies of SWCNTs on the Fe (1 1 1) plane. (a) Assuming the energy of zigzag bond is 0.250 eV. (b) Assuming 0.150 eV.

From these data, interfacial energy difference between armchair bond and zigzag bond is calculated as 0.432 eV by least squares method. Note that, in this system zigzag bonds were more stable than armchair bonds on the Fe catalysts. Relative Gibbs free energies calculated from this energy difference and assuming the zigzag bond energy is 0.250 eV/bond and 0.150 eV/bond are shown in Figs. S1 (a) and (b), respectively. The most stable chirality is (7,0) in the former case and (10,0) in the latter. In both cases (9,0) which is grown in the MD simulation is stable enough to grow.

In addition, we have obtained more chirality definable SWCNTs with 60-mer, 70-mer and 80-mer Co/Fe catalysts in our further ongoing works. We show the all chiralities in Fig. S3. In our results, near-armchair SWCNTs were not stable enough to grow continuously longer than one whole ring consisting of hexagons.

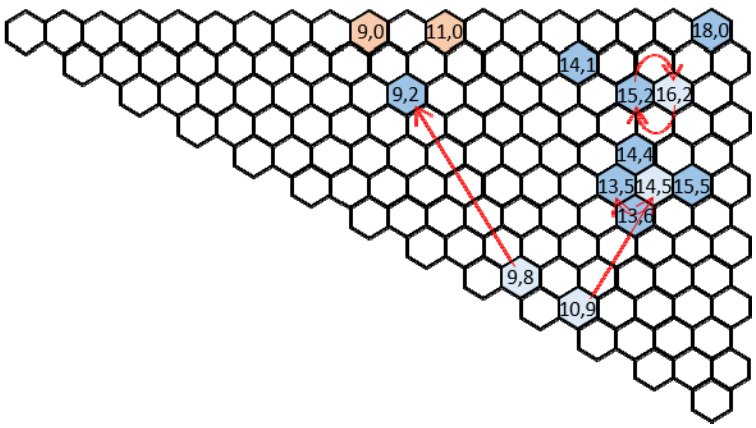

Fig. S3. All chiralities obtained in the MD simulations. The blue hexagons show the chiralities obtained on Co catalysts and the red ones show the chiralities obtained on Fe catalysts. The pale blue ones show that the SWCNTs with the chiralities were not stable and changed into other chiralities.

3. Definition of chirality-defined growth

Next, the "chirality-defined" SWCNT wall must be defined since it was not strictly defined in the main body.

The path of hexagons $\{n_i,m_i\}$ is defined as follows:

$$(n_t, m_t)=(1, 0) \text{ or } (0, 1), \sum_t n_t=n, \sum_t m_t=m \quad (1)$$

Especially the chiral vector $\boldsymbol{C_h}$ is represented as

$$\boldsymbol{C_h} = \sum_{t=1}^{n+m} (n_t\boldsymbol{a_1} + m_t\boldsymbol{a_2}) \quad (2)$$

The (n, m) wall is defined as the set of hexagons each of whose element O has at least one path of hexagons $\{n_i, m_i\}$:

$$\{O|\exists\{n_t, m_t\}\forall k(X_k \in \text{hexagons})\} \quad (3)$$

$$\text{where } \overrightarrow{OX_k} = \sum_{t=1}^{k} (n_t\boldsymbol{a_1} + m_t\boldsymbol{a_2}) \quad (4)$$

This definition is more suitable for near-zigzag wall because in some cases, especially more often in near- and pure-armchair cases, the same hexagons can belong to the walls of different chiralities. Despite this failing, the definition successfully distinguished the walls of different chiralities in the cases shown in the text.

4. Rule of chirality change

Figure S4 shows the diagram of the junction [2] between (15, 2) and (16, 2) SWCNT, shown in the Fig. 6 in the main body. The four points R', S', T' and U', are the midpoints between RC, SD, TA and UB in the original diagram, respectively.

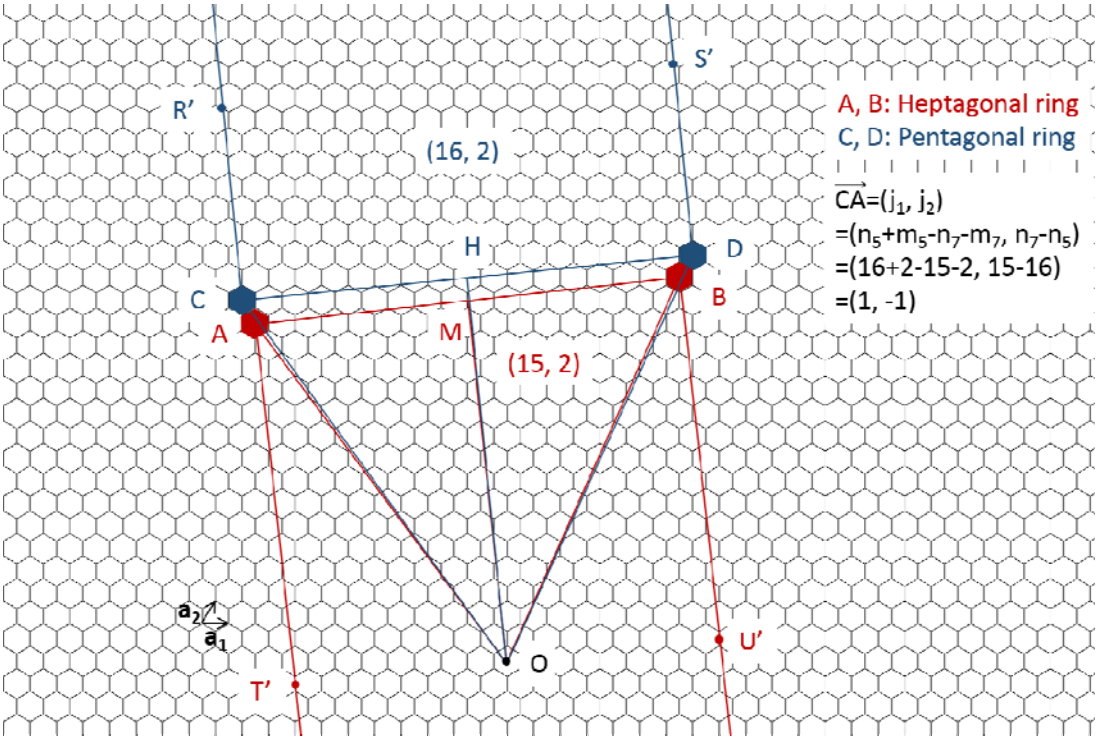

Fig. S4. The junction diagram between (16, 2) and (15, 2).

REFERENCE

1. Magnin, Y.; Amara, H.; Ducastelle, F.; Loiseau, A.; Bichara, C. Entropy-Driven Stability of Chiral Single-Walled Carbon Nanotubes. *Science* **2018**, *362*, 212–215.
2. Saito, R.; Dresselhaus, G.; Dresselhaus, M. S. *Physical Properties of Carbon Nanotubes*; Imperial College Press, 1998.